Physical Biology

OFFICIAL JOURNAL OF
Sociedad de Biofísicos Latino Americanos

PAPER

Protrusion membrane pearling emerges during 3D cell division

To cite this article: David Caballero *et al* 2019 *Phys. Biol.* **16** 066009

Physical Biology

PAPER

Protrusion membrane pearling emerges during 3D cell division

David Caballero[1,2,3,6,7], Inês Mendes Pinto[4], Boris Y Rubinstein[5] and Josep Samitier[1,2,3,6]

[1] Nanobioengineering Group, Institute for Bioengineering of Catalonia (IBEC), The Barcelona Institute of Science and Technology (BIST), Baldiri Reixac 15-21, 08028 Barcelona, Spain
[2] Department of Electronics and Biomedical Engineering, University of Barcelona, C/Martí i Franqués 1, 08028 Barcelona, Spain
[3] Centro de Investigación Biomédica en Red en Bioingeniería, Biomateriales y Nanomedicina (CIBER-BBN), Av. Monforte de Lemos, 3-5, 28029 Madrid, Spain
[4] International Iberian Nanotechnology Laboratory (INL), Avenida Mestre José Veiga, 4715-330 Braga, Portugal
[5] Stowers Institute for Medical Research, Kansas City, MO 64110, United States of America
[6] Author to whom any correspodence should be addressed.
[7] Current address: 3B's Research Group, I3Bs—Research Institute on Biomaterials, Biodegradables and Biomimetics of University of Minho, AvePark—Parque de Ciência e Tecnologia, Zona Industrial da Gandra, 4805-017 Barco, Guimarães, Portugal

E-mail: dcaballero@i3bs.uminho.pt (D C) and jsamitier@ibecbarcelona.eu (J S)

RECEIVED
31 July 2019

REVISED
9 September 2019

ACCEPTED FOR PUBLICATION
17 September 2019

PUBLISHED
10 October 2019

Keywords: cell division, protrusions, pearling, three-dimensions, instability, non-uniformity

Supplementary material for this article is available online

Abstract

Cell division is accompanied by dramatic changes in shape that ultimately lead to the physical separation of one cell into two. In 2D microenvironments, cells round up and remain adhered onto the substrate by thin retraction fibers during division. In contrast, in 3D environments, cells divide exhibiting long protrusions that guide the orientation of the division axis. However, the mechanism of cell division in three dimensions still remains poorly understood. Here we report the spontaneous formation of transient quasiperiodic membrane pearling on extended mitotic protrusions during 3D cell division. Protrusion membrane pearling may be initiated by the non-uniform distribution of focal adhesions and consequent stationary instability of the protrusive membrane. Overall, membrane pearling emergence may provide insights into a novel modality of 3D cell division with potential physiological relevance.

Introduction

Cell division is an essential phenomenon required for several physiopathological processes, including morphogenesis and tumor growth. Despite its unquestionable relevance, it remains widely unknown how cell division is regulated in three-dimensional (3D) environments. The importance of the 3D environment on cell behavior has been widely recognized (Cukierman *et al* 2001, Yamada *et al* 2003, Hakkinen *et al* 2011). Recent evidences have shown that 3D mammalian cell division follows a mechanism and dynamics distinctive from their counterparts on two-dimensional (2D) surfaces (Lesman *et al* 2014, He *et al* 2016, Caballero and Samitier 2017). In 2D, numerous small retraction fibers link the flattened cell to the substrate and spatially determine the division plane (Thery *et al* 2005). As cell division progresses, fibers retraction promotes cell rounding and subsequently the separation of two new daughter cells. In contrast, cells embedded in 3D matrices remain anchored to the matrix throughout the cell division cycle by a small number of long and thin protrusions that orient cell division axis (Lesman *et al* 2014).

An intricate circuitry of intra and extracellular signals regulates cell division. A perturbation of this regulatory mechanism may result in the disruption of protrusions potentially leading to abnormal cell division. Previous studies using planar surfaces showed that cytoskeleton instability artificially induced by the depolymerization of the actin cortex via latrunculin A transformed cell protrusions into a periodic chain of pearl-like structures interconnected by tubes of about 40 nm in diameter (Bar-Ziv *et al* 1999, Heinrich *et al* 2014). In this work, we hypothesized that protrusion transformation (i.e. pearling) could also occur in the absence of cytoskeleton depolymerizing drugs. This transformation would spontaneously occur as a consequence of mechanical instabilities generated from cell-extracellular matrix (ECM) interactions in complex 3D environments. This is of particular interest during 3D cell division, where dividing cells remain anchored

to the ECM by long and thin protrusions (Lesman *et al* 2014). To this end, we used a biomimetic 3D model of the ECM—cell-derived matrices (CDMs)—to monitor and characterize pearling formation and underlie their mechanistic determinants. We combined experimental and theoretical frameworks to infer that non-uniform protrusion adhesion to the surrounding 3D ECM can trigger small-scale perturbations, which eventually lead to the transient formation of pearls distributed quasi-periodically along the protrusion axis. Finally, we hypothesize about the physiological relevance of pearling during 3D cell division, suggesting that pearling might be involved in important physiopathological processes *in vivo*. Altogether, we report a new phenomenon of 3D cell division based on the spontaneous generation of periodic pearling microstructures on extended membrane protrusions, which may provide new insights into the mechanochemical mechanism of 3D cell division.

Material and methods

Cell culture

NIH3T3 mouse fibroblasts (ATCC No. CRL-1658, passage number <20) were grown in high-glucose Dulbecco's Modified Eagle's Medium (DMEM) supplemented with 1% Pen Strep antibiotics (Invitrogen) and 10% bovine calf serum (Sigma) at 37 °C and 5% CO_2. For cell division experiments, cells were trypsinized (0.25% Trypsin-EDTA) (Invitrogen), centrifuged, and seeded on the sample (3D CDM and 2D FN-coated coverslips (CS)) at low density (1–2 $\times$ 10^4 cells·ml^{-1}). Cell culture medium was replaced with fresh medium after 20 min to remove non-adherent cells. Cells were authenticated by regular morphology check by microscope as recommended by the supplier and by using low-passages for the experiments. Mycoplasma contamination was regularly checked by means of commercial kits.

Optical microscopy

Time-lapse cell imaging was performed using an inverted phase-contrast microscope (Olympus IX71) equipped with a CCD camera (Hamamatsu), a 4 $\times$ phase contrast air objective (NA 0.25), and a red filter (Thorslab) to prevent phototoxicity. An environmental chamber (Okolab) was used to maintain physiological conditions (37 °C, 5% CO_2). Image acquisition rate was set at 1 image each 5 min for 24 h. Immunostained cells were visualized using a confocal microscopy (Leica TCS SP5 MP System) equipped with a 20 $\times$ air objective (NA 0.75). Z-stacks separated 0.5 μm were collected, z-projected (Maximal Projection plug-in, Fiji, NIH). Images were pseudo-coloured using a Fire LUT (Fiji, NIH) for eye guidance.

3D ECM model

Glass CS of about 130 μm in thickness and 25 mm in diameter (Ted Pella Inc. #1) were first sterilized under UV for 5 min, activated with O_2 plasma for 30 s, and incubated with 1% gelatin (Sigma) for 1 h at 37 °C. Next, the gelatin-coated CS were rinsed twice with sterile PBS 1 $\times$ and incubated with 1% glutaraldehyde (Sigma) for 20 min at room temperature. The samples were then rinsed twice with PBS 1 $\times$ and incubated with a 1 M glycine (Sigma) PBS 1 $\times$ solution for 30 min at room temperature. Next, the CS were rinsed with PBS 1 $\times$ and DMEM (Invitrogen) supplemented with 10% BCS (Sigma) and 1% Pen Strep (Invitrogen). Finally, 5 $\times$ 10^5 NIH3T3 (ATCC) 'sacrificial' mouse embryonic fibroblasts were seeded on the functionalized CS to initiate CDM growth. NIH3T3 fibroblasts were kept in culture for 8 d adding every other day 50 μg·ml^{-1} of ascorbic acid (A.A.) (Sigma) to favour the generation of collagen. Finally, the sacrificial fibroblasts were removed using extraction buffer (20 mM NH_4OH, 0.5% Triton-X-100 in PBS 1$\times$) (Sigma) to liberate the CDM. The generated matrices were rinsed twice with PBS 1$\times$, and next, with complete cell culture medium. For 2D experiments, glass CS were O_2 plasma activated for 30 s and coated with a 10 μg·ml^{-1} fibronectin (FN) (Sigma) PBS 1$\times$ solution for 1 h at room temperature. The CS were then rinsed with PBS 1$\times$ twice and stored in PBS 1$\times$ at 4 °C before use.

Immunostaining

NIH3T3 cells (ATCC) were fixed with formalin (Sigma) for 20 min at room temperature, permeabilized with 0.5% Triton (Sigma) for 3 min, and finally washed twice with PBS 1$\times$ for 5 min twice. Focal adhesions (paxillin) were stained with mouse anti-paxillin (1:1000) (Thermofisher). Alexa 488 goat anti-rabbit (1:1000) was used as a secondary antibody (Abcam). All the incubations were performed at room temperature for 45 min in PBS 1$\times$ with 3% bovine serum albumin.

Image analysis and biophysical characterization

Pearling formation on extended mitotic protrusions was characterized from the time-lapse movies (Fiji, NIH). We measured the following biophysical parameters: (i) average number of extended protrusions per cell; (ii) percentage of cells with unipolar and bipolar mitotic protrusions; (iii) percentage of cells displaying pearling during division; (iv) pearl lifetime (τ), defined as the time during which the pearls appeared and disappeared; (v) FFT spectrum and pearl spatial period (λ); (vi) pearl diameter (ϕ); (vii) protrusion length; (viii) protrusion width; (ix) pearl interdistance (I), defined as the distance connecting two consecutive pearls; and (x) average number of pearls per protrusion.

Statistical analysis

Unpaired Student's t test was used for statistical significance as indicated in the figure legends. Data are shown as mean $\pm$ standard deviation (S.D.), and

differences were considered statistically significant when $p < 0.05$. The statistical details including the number of experiments and number of cells are included in each figure legend. The total number of cells analyzed were: in 3D CDM, $n_{\text{total}}^{\text{CDM}} = 50$; in 2D FN, $n_{\text{cells}}^{\text{FN}} = 50$) with at least three independent biological repeats.

Results and discussion

3D ECM enhances probability of protrusion formation

Cell-free 3D CDMs were grown on functionalized glass coverslips (CS) for 8 d in the presence of ascorbic acid (figure 1(a) and Methods). The matrices displayed disordered fibrillary structures reminiscent of *in vivo* mesenchymal matrices (Caballero *et al* 2017), with thicknesses of 10–20 μm. This was sufficient to visualize cells embedded within the matrix displaying native-like phenotypes, revealing the 3D nature of the CDMs, as previously reported (Beacham *et al* 2001, Castelló-Cros and Cukierman 2009, Goetz *et al* 2011). This was further confirmed by the visualization of the collagen fibres by second harmonic generation (figure S1 (stacks.iop.org/PhysBio/16/066009/mmedia) and Supplementary Methods). These matrices were rich both in collagen and fibronectin, and with stiffness values of 2–12 kPa (Goetz *et al* 2011). For cell division experiments, NIH3T3 fibroblasts were re-seeded on both the 3D CDM and on 2D FN-coated CS at low cell density and allowed to adhere for 12 h. On 2D FN-coated surfaces, cells displayed the conventional spread—mesenchymal—phenotype with a large front edge and long tail, whereas cells on 3D CDMs displayed a more dendritic and spindle-like phenotype (figure 1(b)). In this case, cells elongated multiple, thin, and long protrusions along the matrix fibres.

During cell division on 2D surfaces, cells rounded up retracting protrusions, but maintaining numerous small retraction fibres, which allowed cells to interact with the substratum (figures 1(c) and S2). After division, the newly formed cells spread and migrated towards the direction set by the mitotic spindle (Thery *et al* 2005). Distinctively, in 3D CDMs, cells rounded up while keeping extended the mitotic protrusions adhered to the CDM all throughout the division process (figure 1(d), arrowheads, and movies S1 and S2). Typically, during 3D cell division, NIH3T3 fibroblasts with mainly two extended protrusions were observed, whereas in 2D this was a rare event (figure 1(e)). However, we also observed a unipolar phenotype during 3D cell division (figures 1(d) and (f)). This phenomenon was not exclusive to the cell used, as it was also observed in other type of fibroblasts (figure S3). These protrusions were recently proposed to guide the orientation of cell division and the migration of newly daughter cells upon cytokinesis in 3D environments (Lesman *et al* 2014). Frequently, a stringent transient rupture of the cell body followed the extended protrusions after rounding (figure 1(d), bottom). This process was highly stochastic and no spatiotemporal order was observed. This rupture, however, did not affect the location or morphology of the extended protrusions, which were strongly tethered on the matrix. Overall, these results indicate that protrusion retraction is not required for cell division in biomimetic 3D microenvironments, where—rounded-up—cells retain extended protrusions during division to orient their division plane.

Pearling emerges on late mitotic protrusions

We next asked whether membrane disruption could also occur along the extended mitotic protrusions. Indeed, we observed the spontaneous formation of discrete and periodic 'pearls' of uniform size all along the mitotic protrusions after cell rounding (figure 2(a) and movie S3). We found that the pearls emerged on late mitotic protrusions. The mitotic pearls were mainly transient and all of them rapidly re-integrated (relaxed) into the plasma membrane resulting into normal (non-pearled) protrusions before completion of the cell division cycle, i.e. before the physical separation of cells. We did not observe any mitotic pearling protrusions breaking up into smaller vesicles. During this period, the pearls were static and did not move along the fibre. Interestingly, we also observed the formation of more stable pearls, which did not re-integrate rapidly into the protrusion membrane (figure 2(b) and movie S4). Note also that other cellular phenomena in 3D, such as cell migration, did not show any pearling formation.

We found that pearling formation was mainly a characteristic of 3D cell division, where most of the cells (~75%) displayed pearling during division (figure 2(c)). In contrast, only a small percentage of cells (<10%) displayed pearl-like structures during division on 2D surfaces. As mentioned above, these pearls were transient and had an average lifetime duration $\tau = 14.4 \pm 5.1$ min, which was about one third of the total division duration (50.1 ± 15.0 min) (figure 2(d)).

The pearls displayed a periodic arrangement demonstrated by the Fast Fourier Transform (FFT) analysis, with a spatial period $\lambda = 7.5 \pm 3.2$ μm and a pearl diameter $\phi = 3.8 \pm 1.3$ μm (figures 3(a)–(c)). Strikingly, we found that on bipolar cells, pearls mainly emerged in one—main—protrusion, with a reduced number of cells displaying pearls also in the secondary protrusion. The main and secondary protrusions were defined as follows: if the dividing cell displayed pearls on a protrusion, then that was defined as the main protrusion, and the secondary protrusion(s) was the one without pearls (figure 3). Interestingly, during this asymmetric cell division, the length and pearl interdistance of both the main and secondary protrusion was similar (figures 3(d), (e)). However, we found a difference in protrusion width (figure 3(f)). We also observed that

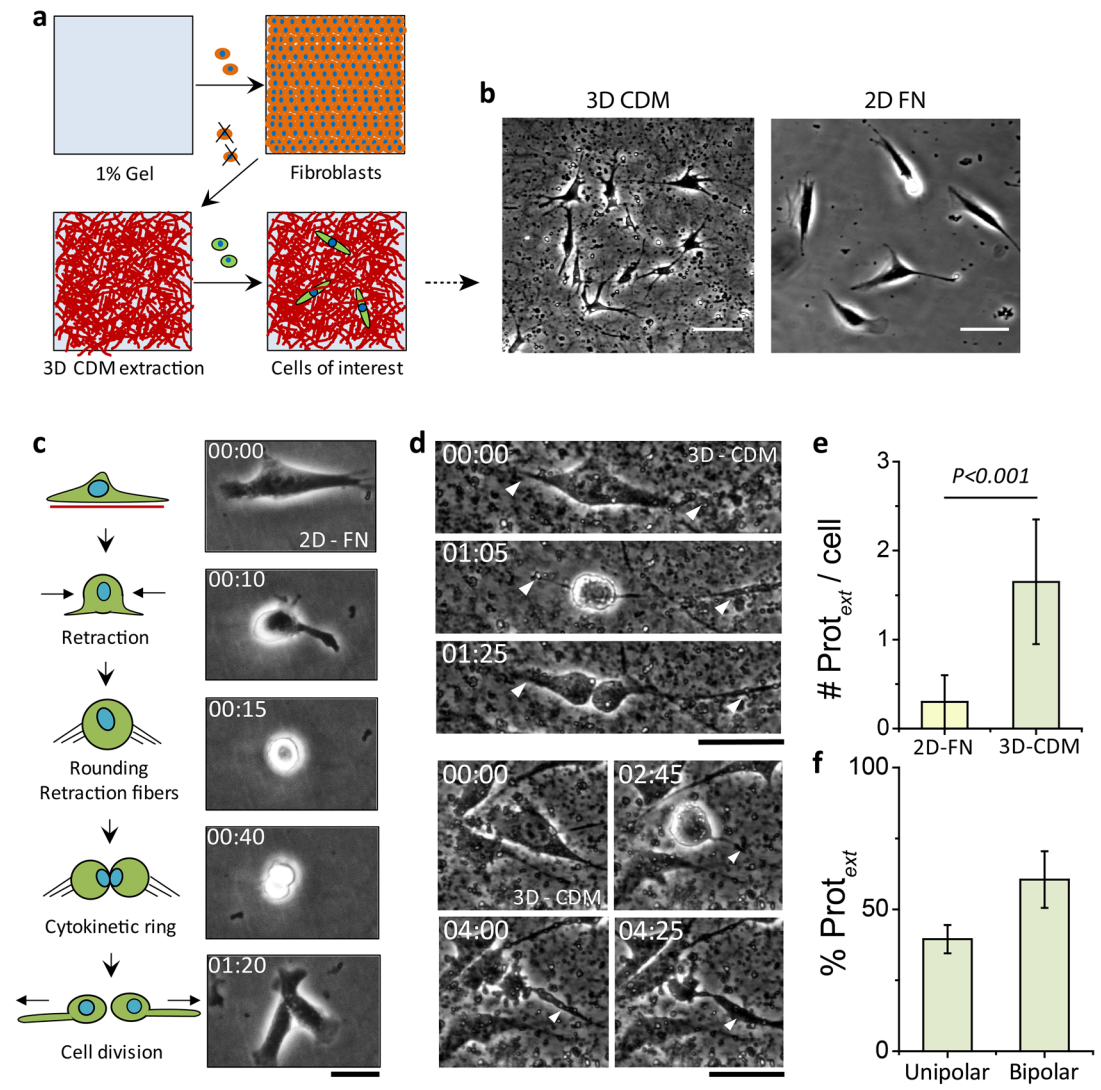

Figure 1. Cells display different phenotypes during cell division in 2D and 3D environments. (a) Scheme showing the fabrication procedure of 3D native-like CDM (Gel: Gelatin). (b) Phase-contrast microscopy images of NIH3T3 fibroblasts seeded on (left) a 3D CDM and (right) on a flat FN-coated surface. Scale bars: 100 μm. (c) and (d) Time-lapse sequence of an NIH3T3 cell dividing on a (c) flat FN-coated surface and (d) 3D CDM. In (d), cells maintained extended (upper) bipolar or (lower) unipolar protrusions throughout the entire cell division process. White arrowheads highlight the extended protrusions during division (see also movies S1 and S2). Scale bars: 50 μm. (e) Quantification of the number of extended—mitotic—protrusions ($Prot_{ext}$) for 2D and 3D conditions. (f) Quantification of the percentage of the number of dividing cells displaying extended unipolar and bipolar protrusions. Data set: $N = 3$ independent biological repeats, $n = 50$ cells per condition. Data: mean $\pm$ S.D. Statistical significance: student's t-test. Time in hh:mm.

the width of protrusions from cells dividing without pearling ($P^{w/o}_{width} = 4.3 \pm 1.4$ μm) was larger than that of cells displaying pearls ($P^{Main}_{width} = 3.0 \pm 1.4$ μm and $P^{Sec}_{width} = 1.8 \pm 0.9$ μm). This suggests that protrusion width change between pearls as previously reported (Heinrich *et al* 2014). Finally, we investigated whether the number of pearls depended on the length of mitotic protrusions. Indeed, we found a good linear correlation between both parameters (figure 3(g)). We measured a mean value of 0.09 ± 0.05 pearls·μm^{-1}. The large uncertainty (~50%) might be related to the difficulty to capture (e.g. out-of-plane or protrusion deformations in z-axis) and measure in a 3D environment the spontaneous formation of pearls and the full length of protrusions. Finally, we also measured the critical protrusion length ($P_{Critical}$) above which pearling started to appear, finding a value of $P_{Critical} \sim 25$ μm (see figure 3(g)). This value can be experimentally explained by considering that the formation of a periodic protrusion with pearls has an average spatial period of $\lambda = 7.5 \pm 3.2$ μm with a minimum of 2–3 pearls. A protrusion with this number of pearls must have a length of 20–30 μm, which provides a phenomenological explanation of the observed $P_{Critical}$. Taken together, these results show that protrusion pearling emerges spontaneously on late mitotic protrusions, and mainly in one—main—protrusion.

Non-uniform tension promotes protrusion static instability and pearling formation

The classical understanding of the pearling formation process arises from studies in 2D surfaces where

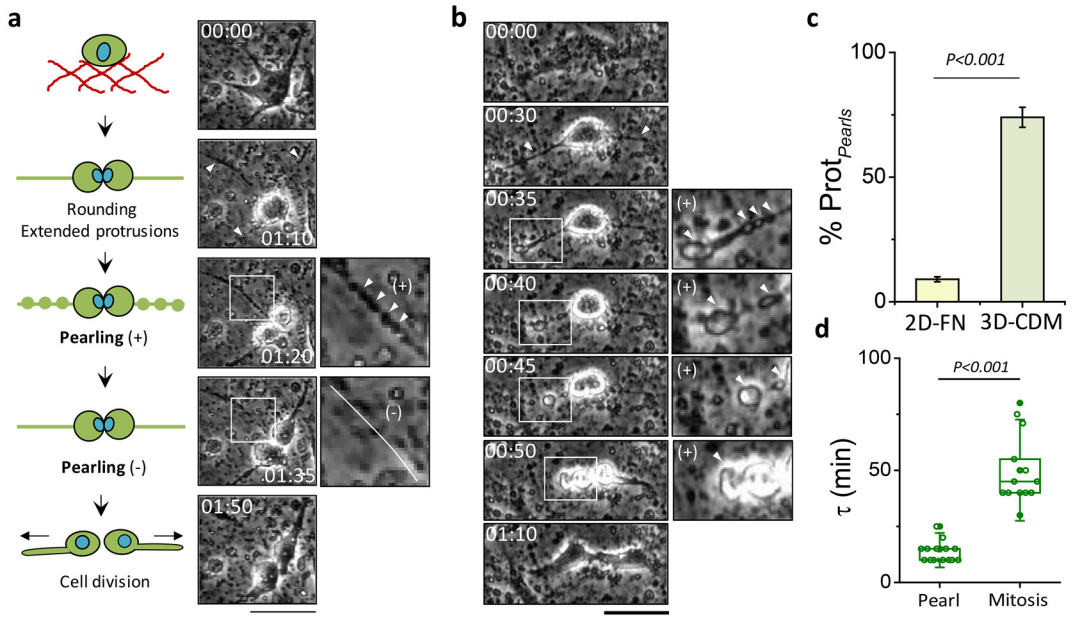

Figure 2. Protrusions pearling during 3D cell division. (a) and (b) Time-lapse sequence of an NIH3T3 fibroblast dividing on a 3D CDM displaying the formation of (a) transient and (b) more stable pearling on extended protrusions (see white arrowheads, and movies S3 and S4). (NOTE: the difference in appearance with the transient pearls is due to an image artefact.) (c) Quantification of the percentage of cells showing the formation of pearl-like structures during 2D and 3D cell division. (d) Pearling lifetime. Scale bars: 50 μm. Data set: $N = 3$ independent biological repeats, $n = 50$ cells per condition. Data: mean $\pm$ S.D. Statistical significance: student's t-test. Time in hh:mm.

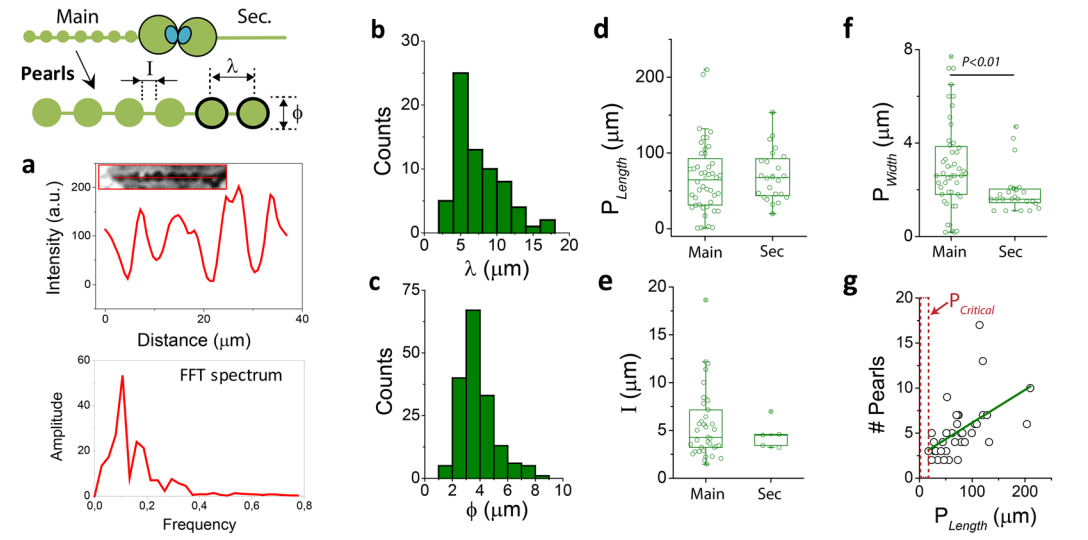

Figure 3. Biophysical characterization of protrusion pearling. The top left scheme displays the different biophysical parameters analyzed. (a) (Upper) Profile of a representative mitotic protrusion (inset image). (Lower) FFT spectrum showing pearl periodicity. (b), (c) Histograms of (b) pearling period λ, and (c) pearl diameter ϕ, respectively. (d)–(f) Quantification of protrusion (d) length (P_{Length}), (e) pearl interdistance (I), and (f) protrusion width (Pwidth) (I) for both the main and secondary (Sec.) protrusions. (g) Correlation between the number of pearls and protrusion length ($R = 0.54$). P_{critical} (~25 μm) indicates the value above which pearling started to appear. Data set: $N = 3$ independent biological repeats, $n = 50$ cells per condition. Statistical significance: Student's t-test.

pearling is described as a result of a stationary instability generated in an actin-based protrusion upon pharmacological reduction of its rigidity (Bar-Ziv *et al* 1999). Even though this previous study was conducted on 2D surfaces, it is important to note that a protrusion with pearls is a 3D object. We believe that a similar mechanism may be responsible for pearling emergence during 3D cell division, but importantly, in the absence of pharmacological drugs, and it can be understood as follows. Considering an elastic cylindrical tube of a constant cross section radius $R(x) = R0$ (figure 4(a)), a random perturbation of the tube radius with the amplitude $dR(x) \ll R0$ emerges at position x along the tube axis, so that the radius is given by $R(x) = R0 + dR(x)$. If the tube is very rigid this perturbation cannot grow and eventually disappears, so that the original shape of the tube remains unchanged. When the flexibility increases, this small

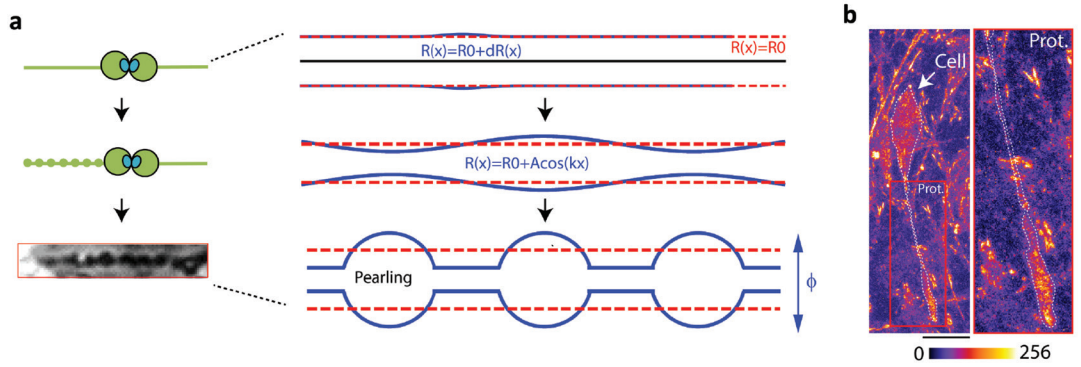

Figure 4. Mechanism of pearling formation. (a) Non-uniform tension resulting from an uneven adhesion between the protrusion tube and the ECM promotes random small scale perturbations in the actin tube radius $R(x)$ in the form of $R(x) = R0 + \mathrm{d}R(x)$. This initial perturbation grows and leads to the formation of a structure described by the shape of a periodic function $R(x) = R0 + A \cdot \cos(k \cdot x)$. The growth of the perturbation continues resulting in a non-linear structure made of pearls separated by cylindrical-shaped segments. (b) Confocal microscopy image of a dividing NIH3T3 fibroblast stained for paxillin (pseudo-coloured—Fire LUT—for eye guidance). The image shows the non-uniform distribution of paxillin along the protrusion axis prior to pearling formation. Right panel shows a magnified image of the highlighted region. White dashed line determines the contour of the cell and extended protrusion. Scale bar: 50 μm.

perturbation grows and eventually takes the shape of periodic function $\mathrm{d}R(x) = A \cdot \cos(k \cdot x)$, where the amplitude A and the wave number k (inverse of the wavelength $k = 2\pi/L$) depend on the tube parameters. Thus, a new quasi-stable profile $R(x) = R0 + A \cdot \cos(k \cdot x)$ is formed, but the growth of the perturbation does not stop. Eventually, the radius $R(x)$ of the profile along the tube axis approaches the characteristic non-linear shape where nearly spherical pearls are separated by segments well approximated by the cylinders (figure 4(a)) (Bar-Ziv and Moses 1994, Heinrich *et al* 2014). The pearl interdistance in such a model remains constant and depends on the tube flexibility.

We note that the instability mechanism described above is a combination of surface tension and local curvature of the membrane. Similar factors play important role in the furrow ingression mechanism discussed in refs. (Zhang and Robinson 2005, Poirier *et al* 2012, Robinson *et al* 2012). It should be underlined that this kind of instability is self-organized as it is initiated by a random radial perturbation. This means that pearl shape and spacing is not imposed by any external periodic process or structure but depends only on the tube parameters. On the other hand, the initial random perturbation, its position, or amplitude are affected by external processes, such as the interaction of the cell with the extracellular environment. In this regard, we hypothesized that the initiation of the pearling formation (in the absence of drugs) may be related to the non-uniformity of protrusion adhesion to the 3D ECM along the protrusion axis. In consistency with this hypothesis, figure 4(b) shows NIH3T3 cells with a heterogeneous distribution of paxillin along the mitotic protrusion. Such non-uniformity can trigger initial small-scale perturbations in the tube cross section radius, which progresses and eventually leads to formation of a quasi-periodic non-linear pearling structure. This non-uniform distribution of focal adhesions along the protrusion can contribute to the initiation of the pearling formation, but not to the outcome of the pearling process. Note that other processes that may contribute to the initiation of the pearling are traction force fluctuations of focal adhesions (Plotnikov *et al* 2012, Wu *et al* 2017). Finally, it should be also noted that if the tube flexibility changes with time, the pearl structure may disappear when the flexibility decreases sharply. This factor can explain the finite lifetime τ of pearls. When the division is over and cells separate physically, the long mitotic protrusions start to shrink. Then, the number of pearls decreases until they completely disappear. Therefore, the protrusion length limits pearling lifetime.

We next investigated whether the pharmacological inhibition of the Rho-pathway, ROCK and Myosin II motor could affect pearling formation in 3D cell division. Live cell imaging did not show any significant formation of pearling during division suggesting that actomyosin contractility is potentially important for pearling formation as the source of variation in tension that leads to instabilities.

Finally, it is important to stress that even though the appearance of pearling is not an exclusive phenomenon of 3D cell division, it does require the formation of elongated cylindrical tubes (i.e. protrusions), that might undergo pearling. Other cellular processes in 3D are lacking these structures thus eliminating the possibility of pearling. At this stage, the functional role of pearling in the mechanism of 3D cell division is speculative. Even though the formation of pearls is not a requirement for the cell division in 3D, as cells can divide even in the absence of pearling, it may have important implications in fundamental physiopathological processes, such as embryonic development or cancer dissemination. Indeed, the appearance of pearls in more complex tubular systems, such as arteries, renal, or intestinal tubes, is at the origin of many pathologies (Buechner *et al* 1999, Peynircioglu and Cil

2008, Hannezo *et al* 2012). Future studies including high resolution image characterization of the molecular players, e.g. F-actin or reticular adhesions (Lock *et al* 2018), may be therefore needed to assess its physiological relevance *in vivo*.

Conclusions

In conclusion, we report a novel 3D-specific phenomenon during cell division, where NIH3T3 fibroblasts seeded in 3D CDMs undergo division maintaining extended mitotic protrusions throughout the entire division cycle and showing the appearance of transient membrane pearls along these protrusions. Interestingly, the division is asymmetric with the appearance of pearling mainly in one—main—of the mitotic protrusions. The mechanism of membrane pearling is currently a subject of intense experimental and theoretical studies (Hannezo *et al* 2012, Heinrich *et al* 2014, Jelerčič and Gov 2015). In membrane tubes similar to cellular protrusions, pearling has been associated to an instability caused by a competition between curvature and surface tension (Bar-Ziv and Moses 1994). Here, we describe transient pearls as a consequence of the development of stationary instability partially driven by non-uniformity of the adhesion to the ECM, which triggers small-scale perturbations that lead to the formation of pearls distributed quasi-periodically along the protrusion axis. However, we do not exclude the existence of intracellular-based mechanisms controlling non-uniform tension and pearling formation.

Acknowledgments

DC acknowledges the support of the Secretary for Universities and Research of the Ministry of Economy and Knowledge of the Government of Catalonia and the COFUND program of the Marie Curie Actions of the European Union's Seventh R&D Framework Program (BP-DGR 2013). The Nanobioengineering Group has support from the Commission for Universities and Research of the Department of Innovation, Universities, and Enterprise of the Generalitat de Catalunya (2014 SGR 1442). IMP acknowledges the financial support from the Marie Curie COFUND Programme 'NanoTRAINforGrowth', from the European Union's Seventh Framework Programme for research, technological development and demonstration under grant agreement no 600375. This article is a result of the project 'Advancing cancer research: from basic knowledge to application' (NORTE-01-0145-FEDER-000029), co-financed by Norte Portugal Regional Operational Programme (NORTE 2020), under the PORTUGAL 2020 Partnership Agreement, through the European Regional Development Fund (ERDF).

Author contributions

Conceptualization: DC and IMP; Investigation: DC, IMP and BYR; Visualization: DC; Data Analysis: DC, IMP and BYR; Theoretical Description: IMP and BYR; Writing & Editing: DC, IMP, BYR and JS; Overall Supervision and Funding Acquisition: DC and JS

Conflicts of interest

There are no conflicts to declare.

ORCID iDs

David Caballero https://orcid.org/0000-0001-7930-2535
Ines Mendes Pinto https://orcid.org/0000-0002-8009-7767

References

Bar-Ziv R and Moses E 1994 Instability and 'pearling' states produced in tubular membranes by competition of curvature and tension *Phys. Rev. Lett.* **73** 1392–5
Bar-Ziv R, Tlusty T, Moses E, Safran S A and Bershadsky A 1999 Pearling in cells: a clue to understanding cell shape *Proc. Natl Acad. Sci. USA* **96** 10140–5
Beacham D A, Amatangelo M D and Cukierman E 2007 Preparation of extracellular matrices produced by cultured and primary fibroblasts *Curr. Prot. Cell Biol.* **33** 10.9.1–10.9.21
Buechner M, Hall D H, Bhatt H and Hedgecock E M 1999 Cystic canal mutants in caenorhabditis elegans are defective in the apical membrane domain of the renal (excretory) cell *Dev. Biol.* **214** 227–41
Caballero D, Palacios L, Freitas P P and Samitier J 2017 An interplay between matrix anisotropy and actomyosin contractility regulates 3D-directed cell migration *Adv. Funct. Mater.* **27** 1702322
Caballero D and Samitier J 2017 Topological control of extracellular matrix growth: a native-like model for cell morphodynamics studies *ACS Appl. Mater. Interfaces* **9** 4159–70
Castelló-Cros R and Cukierman E 2009 Stromagenesis during tumorigenesis: characterization of tumor-associated fibroblasts and stroma-derived 3D matrices *Methods Mol Biol.* **522** 275–305
Cukierman E, Pankov R, Stevens D R and Yamada K M 2001 Taking cell-matrix adhesions to the third dimension *Science* **294** 1708–12
Goetz J *et al* 2011 Biomechanical remodeling of the microenvironment by stromal caveolin-1 favors tumor invasion and metastasis *Cell* **146** 148–63
Hakkinen K M, Harunaga J S, Doyle A D and Yamada K M 2011 Direct comparisons of the morphology, migration, cell adhesions, and actin cytoskeleton of fibroblasts in four different three-dimensional extracellular matrices *Tissue Eng. A* **17** 713–24
Hannezo E, Prost J and Joanny J-F 2012 Mechanical instabilities of biological tubes *Phys. Rev. Lett.* **109** 018101
He L, Chen W, Wu P-H, Jimenez A, Wong B S, San A, Konstantopoulos K and Wirtz D 2016 Local 3D matrix confinement determines division axis through cell shape *Oncotarget* **7** 6994–7011

Heinrich D, Ecke M, Jasnin M, Engel U and Gerisch G 2014 Reversible membrane pearling in live cells upon destruction of the actin cortex *Biophys. J.* **106** 1079–91

Jelerčič U and Gov N S 2015 Pearling instability of membrane tubes driven by curved proteins and actin polymerization *Phys. Biol.* **12** 066022

Lesman A, Notbohm J, Tirrell D A and Ravichandran G 2014 Contractile forces regulate cell division in three-dimensional environments *J. Cell Biol.* **205** 155–62

Lock J G, Jones M C, Askari J A, Gong X, Oddone A, Olofsson H, Göransson S, Lakadamyali M, Humphries M J and Strömblad S 2018 Reticular adhesions are a distinct class of cell-matrix adhesions that mediate attachment during mitosis *Nat. Cell Biol.* **20** 1290–302

Peynircioglu B and Cil B E 2008 Standing waves of hepatic artery associated with renal and extrarenal fibromuscular dysplasia *Cardiovasc. Intervent. Radiol.* **31** 38–40

Plotnikov S V, Pasapera A M, Sabass B and Waterman C M 2012 Force fluctuations within focal adhesions mediate ECM-rigidity sensing to guide directed cell migration *Cell* **151** 1513–27

Poirier C C, Ng W P, Robinson D N and Iglesias P A 2012 Deconvolution of the cellular force-generating subsystems that govern cytokinesis furrow ingression *PLoS Comput. Biol.* **8** e1002467

Robinson D, Kee Y, Luo T, Surcel A and Egelman E 2012 Understanding how dividing cells change shape *Comprehensive Biophysics* vol 7, ed E H Egelman (Oxford: Academic) pp 48–72

Thery M, Racine V, Pepin A, Piel M, Chen Y, Sibarita J-B and Bornens M 2005 The extracellular matrix guides the orientation of the cell division axis *Nat. Cell Biol.* **7** 947–53

Wu Z, Plotnikov S V, Moalim A Y, Waterman C M and Liu J 2017 Two distinct actin networks mediate traction oscillations to confer focal adhesion mechanosensing *Biophys. J.* **112** 780–94

Yamada K M, Pankov R and Cukierman E 2003 Dimensions and dynamics in integrin function *Braz. J. Med. Biol. Res.* **36** 959–66

Zhang W and Robinson D N 2005 Balance of actively generated contractile and resistive forces controls cytokinesis dynamics *Proc. Natl Acad. Sci. USA* **102** 7186–91